Customized Coordinated Voltage Regulation and Voyage Scheduling for All-Electric Ships in Seaport Microgrids

Xianzhuo Sun, *Member, IEEE,* Jing Qiu, *Senior Member, IEEE,* Yuechuan Tao, *Member, IEEE,* Huichuan Liu, and Junhua Zhao, *Senior Member, IEEE*

***Abstract*—This paper proposes a customized coordinated voltage regulation and voyage scheduling strategy for all-electric ships (AES) to find a trade-off between minimizing operation cost during cruising and reducing power losses of microgrids, which also guarantees system voltage security. Based on a predefined sea route with minimum added resistance, the optimal voyage scheduling is first performed to achieve energy management and speed adjustment of AES. This process also obtains multiple AES arrival time-state of charge (T_a-SOC_a) pairs and sends them to the microgrid central controller (MGCC). The MGCC then performs optimal voltage regulation to minimize power losses through the dispatch of on-load tap changers (OLTC), photovoltaic inverters (PVs) and berthed-in AES. The voltage regulation model is an extension of the conventional volt/var optimization by incorporating berth allocation problems and T_a-SOC_a constraints. To achieve effective solutions, both the voyage scheduling and voltage regulation problems are converted to mixed-integer linear programs (MILP) with linearization methods. Moreover, a customized coordinated optimization procedure embedded with a satisfactory index (SI) is proposed to solve the problem, which helps select T_a-SOC_a pairs for each AES and ensures an acceptable operation cost during the voyage scheduling. The simulation results verify that the proposed method achieves secure and optimal operation in seaport microgrids. It can also find a trade-off between minimizing the operation cost of AES and reducing power losses in microgrids.**

***Index Terms*—Customized coordinated voltage regulation and voyage scheduling, all-electric ships, seaport microgrids, berth allocation, T_a-SOC_a pairs**

NOMENCLATURE

A. Sets/Indices

ij, E	Index and set of branches in microgrids
k, A	Index and set of AES
m, B	Index and set of berths at the seaport
t, T	Index and set of time periods

B. Parameters

α_0, α_1, α_2	Coefficients of battery lifetime function
ρ_1, ρ_2	Coefficients of propulsion power function
$\delta_{m,k}$	Berthing time of k^{th} AES at m^{th} berth
η_{ch}, η_{dis}	Charging/discharging efficiency of ESS
c_0, c_1, c_2	Fuel cost coefficients of DSG on AES
$E_{\text{ESS},k}$, S_{PV}	Rated capacity of ESS and PVs
M	A large positive number
$P^{\min}_{\text{DSG},k}$, $P^{\max}_{\text{DSG},k}$	Lower/upper bounds of DSG generation
$P^{\min}_{\text{dis},k}$, $P^{\max}_{\text{dis},k}$	Lower/upper bounds of ESS discharging power
$P^{\text{ramp}}_{\text{DSG},k}$	Ramp rate limit of DSG on AES
$P_{EPC,m,t}$	Active power supply to EPC at each berth
r_{ij}, x_{ij}	Resistance/reactance of branch ij
$SOC^{\min/\max}$	Lower/upper bounds of SOC of ESS
$tap^{\max}$	Maximum daily switching times of OLTC
$TC_{\text{ESS},k}$	Total investment cost of ESS
$V^{\min}$, $V^{\max}$	Lower/upper bounds of bus voltages
$v_t^{\min}$, $v_t^{\max}$	Lower/upper bounds of AES velocity
V_s, ΔV_T	Primary side/per-step voltage of OLTC

C. Variables

$\omega_{m,k,t}$	Binary indicator, =1 if k^{th} AES is served at m^{th} berth at time t, =0 otherwise
$\mu_{m,k,t}$	Binary indicator, =1 if m^{th} berth starts serving k^{th} AES at time t, =0 otherwise
$\lambda_{k,j}$, γ_t, $x_{m,k,t}$	Auxiliary variables used in linearization
β_k	A threshold customized by each AES user
$a_{k,j}$, $b_{k,j}$	Slope and y-axis intercept of piecewise

This work was supported by the ARC Research Hub Grant IH180100020, the ARC Training Centre IC200100023, the ARC linkage project LP200100056 and the ARC DP220103881. This work was also supported by PolyU research grants No. 1-W29V. The corresponding authors are Jing Qiu and Junhua Zhao.

X. Sun is with the Department of Electrical and Electronic Engineering and the Research Institute of Smart Energy, The Hong Kong Polytechnic University, Hong Kong SAR, China. (Email: xianzsun@polyu.edu.hk).

J. Qiu and H. Liu are with the School of Electrical and Information Engineering, The University of Sydney, Sydney, NSW 2006, Australia. (Email: qiujing0322@gmail.com; huichuan.liu@sydney.edu.au).

Y. Tao is with the School of Electrical and Electronic Engineering, Nanyang Technological University, Singapore. (Email: yuechuan.tao@sydney.edu.au).

J. Zhao is with the School of Science and Engineering, The Chinese University of Hong Kong, Shenzhen, Shenzhen, 518100, China, and also with Shenzhen Institute of Artificial Intelligence and Robotics for Society (AIRS). (zhaojunhua@cuhk.edu.cn).

	linear functions
C_k	Total operation cost of AES
$C_{\mathrm{ESS/DSG},k,t}$	Generation cost of ESS and DSG on AES
$D_{\mathrm{ESS},k,t}$	Depth of discharge of ESS
d_{route}	Total cruising Distance of AES
f_{ij}, f_t	Added resistance along the sea route
$L_{\mathrm{ESS},k,t}$	Battery lifetime as a function of DOD
$P_{\mathrm{dis},k,t}$	Discharging power of ESS during cruising
$P_{\mathrm{DSG},k,t}$	Power generation of DSG on AES
$P_{\mathrm{pl},k,t}$	Propulsion power of AES at time t
$P_{\mathrm{sv1},k,t}$, $P_{\mathrm{sv2},k,t}$	Service load of AES during the cruising and berthing processes
$P_{\mathrm{PV/L},i,t}$,$Q_{\mathrm{PV/L},i,t}$	Active and reactive powers of PV/load
$P_{ij,t}$, $Q_{ij,t}$	Active and reactive powers along branch *ij*
$P_{\mathrm{S},i,t}$	Total charging demand at the port bus
$P_{\mathrm{ch},m,k,t}$	Charging power of a berthed-in AES
SI_k	Customized satisfactory index of AES
$SOC_{k,t}$	SOC values of ESS on AES
$SOC_{a,k}$	SOC of ESS once AES arrives at seaport
tap_t	Tap position of OLTC at slack bus
$T_{s,k}$, $T_{a,k}$, $\mathrm{T}_{b,k}$, $\mathrm{T}_{f,k}$	Start cruising/seaport arrival/start berthing/service completion times of AES
$V_{i,t}$	Bus voltage in seaport microgrids
$v_{k,t}$	Cruising velocity of AES

D. Abbreviation

AES	All-electric ships
GHG	Greenhouse gas emission
DSG	Diesel generator
MGCC	Microgrid central controller
EPC	Electrical port cranes
MILP	Mixed-integer linear program
SOC	State of charge
SI	Satisfactory index
OLTC	On-load tap changer
OPF	Optimal power flow
ESS	Energy storage system
DOD	Depth of discharge
MIQP	Mixed-integer quadratic program

I. INTRODUCTION

ALL-ELECTRIC ships (AESs) are growing steadily as a promising approach to reducing greenhouse gas (GHG) emissions in today's maritime transportation [1]. Compared with traditional diesel-driven vessels, AES equipped with diesel generators (DSG) and energy storage systems (ESS) makes a voyage more flexible [2]. When berthing at the seaport, AES must shut down their DSG and receive onshore power supply to further reduce GHG emissions, namely the "cold-ironing" technology [3]. However, the electric propulsion technology can complicate the operation of AES, while uncoordinated voyage scheduling and "cold-ironing" processes also impose great challenges on the optimal operation of seaport microgrids [4].

Considering a complete voyage from one port to another, the AES plans a sea route, performs voyage scheduling and arrives (berths) at the seaport to receive charging and cargo handling services. The optimal route planning problems have been well studied in [5]-[7] and will not be discussed in detail in this paper. After obtaining an optimal sea route, the AES performs optimal voyage scheduling to minimize the total operation cost under various constraints. In [7], a coordinated voyage scheduling and generation scheduling method is proposed to optimize the sea route, cruising speed and total operation cost of AES in three sequential phases. In [8], an optimal demand-side management and generation scheduling method is proposed to minimize the ship power system operation cost while satisfying GHG emissions constraints. By treating the GHG mitigation as a separate objective, Ref. [9] extends the voyage scheduling problem to a multi-objective optimization which is solved by the nondominated sorting genetic algorithm II. Refs. [10]-[11] propose a two-stage robust optimal voyage scheduling model to address multiple uncertainties, such as uncertain wave and wind and uncertain PV generation caused by moving and swing of AES. Ref. [12] proposes a two-stage coordinated voyage scheduling framework to address the shore-side electricity price variations based on deep-learning forecasting methods.

In addition to the voyage scheduling process, extensive electrification of maritime transportation also lies in the charging process to AES at seaport microgrids. In terms of voltage regulation, seaport microgrids are a newly proposed concept with two distinct differences compared to land-based microgrids. Firstly, seaport microgrids are responsible for providing charging power to berthed-in AES, which can cause heavy load demand at the port bus and increase voltage violation risks. For land-based microgrids, voltage regulation is usually performed in a centralized or local manner to reduce network power losses while mitigating voltage violations. In [13]-[14], centralized control schemes are developed in the microgrid central controller (MGCC) to realize optimal energy management and voltage regulation in microgrids. In [15], a local droop-based primary control method is proposed to achieve precise voltage regulation while securing system reliability in DC microgrids. To incorporate the "cold-ironing" of AES into seaport microgrid operation, Ref. [16] proposes a multi-agent power management method aiming at maximizing the flexibility of seaport power demand, which includes refrigerated containers, electric vehicles and power supply to AES. Secondly, the seaport will allocate a berth position and assign several electrical port cranes (EPC) to a berthed-in AES.

This process, namely berth allocation, can also induce varying charging demand in different time periods and affect the voltage regulation in seaport microgrids. In [17], a simultaneous berth-crane allocation model is proposed to minimize the total waiting and cargo handling times of AES. In [18], the berth allocation model is formulated as a mixed-integer linear program (MILP) and solved by the particle swarm optimization algorithm to achieve efficient solutions. In [19], the MILP berth allocation model is solved by a rolling horizon heuristic and a branch and cut algorithm, which provides good feasible solutions for large-scale systems. In recent research [20]-[22], the berth allocation model is incorporated into microgrid optimal operation problems to coordinate both the electric and logistic sides of the seaport. Ref. [20] formulates an integrated energy system scheduling model accounting for the operating flexibility of berth allocation, reefer area and cold-ironing at the seaport. Ref. [21] proposes a two-stage joint scheduling model under uncertainty, where the first stage performs berth allocation to minimize the time cost of AES and the second stage conducts energy management to minimize operation cost in microgrids. Ref. [22] proposes a distributed optimal voltage regulation and berth allocation model to balance the benefits of microgrid operators and AES based on the alternating direction method of multipliers.

In the above literature, it can be found that the voyage scheduling of AES and voltage regulation of seaport microgrids are usually considered as two separate stages without coordination. The existing research mainly focuses on the coordination between voyage planning and energy management of AES [7]-[12] and the coordination between energy management of microgrids and berth allocation of AES [20]-[24]. They simply formulate the power balance constraints at the port bus and ignore potential adverse impacts of voyage scheduling on the optimal voltage regulation of microgrids, therefore lacking coordination between the two stages. Specifically, the optimal voyage scheduling would result in uncoordinated arrival times and state of charge (SOC) levels of AES, which induces heavy charging demand at the port bus and further causes extra power losses and severe voltage violations. In the previous work [25], a hierarchically coordinated voltage control framework is proposed to improve voltage profiles in seaport microgrids through the voyage scheduling and local charging power control of AES. In this method, the arrival times of AES are designed only to improve voltage security in seaport microgrids, which may in turn increase the operation cost of AES to unacceptable levels. Therefore, it cannot achieve the coordination that finds a trade-off between the operation cost of AES and power losses of microgrids. Furthermore, uncoordinated berth allocation of AES may lead to undesired charging demand and threaten the voltage security of microgrids, which is also ignored in [25]. Under the premise of meeting berthing time requirements, AES and microgrid operators can cooperate to improve voltage control performance. However, incorporating berth allocation into voltage regulation in a cooperation mode receives little attention. To fill the existing research gaps, this paper proposes a customized coordinated voltage regulation and voyage scheduling strategy for AES in seaport microgrids. The major contributions in this paper can be summarized as follows:

(1) We propose a coordinated optimal voltage regulation and voyage scheduling framework for AES. Different from [25] that improves microgrid voltage security at the expense of unacceptable high operation costs of AES, the coordinated optimization framework can achieve "real coordination", i.e., finding a trade-off between reducing the operation cost of AES and minimizing power losses in microgrids with secure voltage levels.

(2) We propose an extended voltage regulation model by incorporating berth allocation into the volt/var optimization in seaport microgrids. Compared to existing models in [20]-[24], this model makes an improvement in the following two aspects. On the one hand, the arrival times of AES are formulated as flexible variables and corresponding nonconvexities are linearized for efficient solutions. On the other hand, the berthing times of AES only follow time frame constraints instead of being minimized. The flexibility in arrival and berthing times fully exploits the voltage regulation capability of AES.

(3) We propose a customized coordinated optimization procedure as the solution methodology for the coordinated optimization problem. The arrival time-SOC (T_a-SOC_a) pairs and satisfactory index (SI) of AES are designed and embedded into the optimization process. By sequentially solving voyage scheduling and voltage regulation problems and carefully selecting T_a-SOC_a pairs based on customized SI, a balance of interests between AES and microgrids will be finally achieved.

II. Coordinated Voltage Regulation and Voyage Scheduling Framework

The proposed coordinated voltage regulation and voyage scheduling framework for AES is presented in Fig. 1. The whole framework is divided into two sequentially coordinated stages, which are voyage scheduling of AES and voltage regulation in seaport microgrids respectively. The seaport microgrids are assumed to operate in the grid-connected mode in this paper. The extension of the proposed method to islanded microgrids is available if there are sufficient power generation resources to balance the charging demand of AES. In the voyage scheduling phase, the route planning of vessels is first determined to minimize total sea resistance from the starting point (S) to the destination (D) with varying sea conditions. By integrating vessel speed and propulsion power constraints into energy management on AES, optimal voyage scheduling is then carried out to minimize the generation costs of DSG and ESS during cruising. This process also obtains multiple T_a-SOC_a pairs for each vessel, which are sent to the MGCC. In the voltage regulation phase, with the day-ahead prediction of PVs and load and T_a-SOC_a pairs, the MGCC performs optimal power flow (OPF) to dispatch voltage control devices and allocate berths/EPC to berthed-in AES. This model is an extension of the traditional OPF in microgrids, which includes not only volt/var optimization of on-load tap changer (OLTC) and PVs but also the berth allocation and charging power models of AES. Note that both the voyage scheduling and voltage regulation processes are performed with an hour resolution ahead of the day.

It is observed that the time and SOC once AES arrives at the seaport build the bridge between the voyage scheduling and voltage regulation. For example, the voyage scheduling results in different values of T_a and SOC_a, which determine the hourly charging power of berthed-in AES and further affect the optimal operation in seaport microgrids. The "coordination" of the proposed method aims to find a trade-off between the operation cost of AES and power losses in microgrids with secure voltage levels. This goal motivates the design of a customized coordinated optimization procedure with a SI of AES, which will be discussed in detail in Section V.

In practice, time schedules and berth allocations of AES are usually predefined and strict due to various constraints on the logistic side, which brings difficulties in the real-life implementation of the proposed method. To this end, more efforts are needed to achieve coordination among multiple parties, including AES, microgrid operators and logistic companies. For example, additional constraints can be added on the start berthing times of AES to meet logistic requirements for cargo transportation. If all parties involved can reach an agreement on time schedules and berth allocations through negotiation, the proposed method will be allowed under real field conditions in the future.

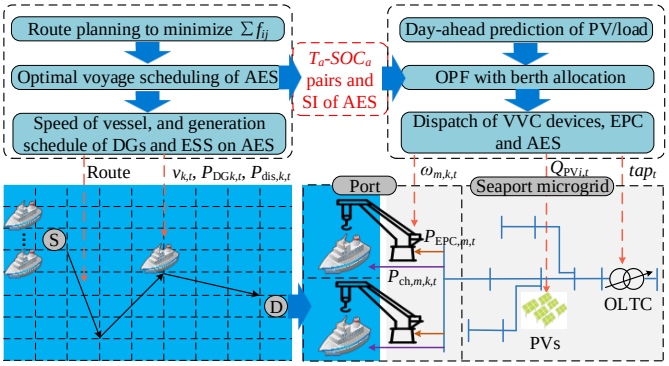

Fig. 1. Coordinated voltage regulation and voyage scheduling framework for AES

III. Optimal Voyage Scheduling of AES

A. Route Planning with Sea Resistance

The vessel route planning aims to find a path with the least sea resistance when cruising to the seaport. Generally, sea resistance is highly related to sea conditions, which can be described by wind speed, wave height, wave length and weather direction angle [10]. Table I presents an empirical Beaufort scale that describes the relationships between the added resistance of AES and sea conditions with varying wind speeds and wave heights. It is observed that lower wind speed and wave height correspond to a flatter sea condition with less resistance, and vice versa. Based on this relationship, route navigation can be formulated as an optimization problem to minimize the total added resistance of a path, as illustrated in (1) and (2) [7].

$$\min \sum_{(i,j)=(1,1)}^{(i,j)=(n,n)} f_{ij}, \forall f_{ij} \in F \tag{1}$$

$$F = \begin{bmatrix} f_{11} & \cdots & f_{1j} & \cdots & f_{1n} \\ \vdots & \ddots & \vdots & \ddots & \vdots \\ f_{i1} & \cdots & f_{ij} & \cdots & f_{in} \\ \vdots & \ddots & \vdots & \ddots & \vdots \\ f_{n1} & \cdots & f_{nj} & \cdots & f_{nn} \end{bmatrix} \tag{2}$$

where f_{ij} is the added resistance when a vessel passes through the coordinate (i,j); f_{11} and f_{nn} are the starting point and destination of the vessel. Note that f_{ij} is assigned to be ∞ if coordinate (i,j) is unreachable from other coordinates. According to [7], [17], the optimization problem can either be solved by dynamic programming or the Dijkstra algorithm to identify the potential sea route and voyage distance. The optimal route planning is adopted to find the path with minimum sea resistance, thereby reducing the propulsion power and operation cost of AES in the following voyage scheduling problem. The time schedules of AES will then be met by adjusting cruising velocity under the optimal route. Note that conducting route planning a priori does not contradict to predefined time schedules of AES, while it also helps complete the voyage scheduling framework.

Table I. Beaufort Scale with added resistance

Beaufort Scale	Wind Speed (knots)	Wave Height (m)	Sea Condition	f ($\leqslant$)
0	<1	0	Flat	0.00
1	1-3	0.1-0.2	Ripple without Crest	0.06
2	4-6	0.3-0.5	Small Wavelet	0.13
3	7-10	0.6-1.0	Large Wavelet	0.20
4	11-16	1.5	Small Wave	0.26
5	17-21	2.0	Moderate Wave	0.33
6	22-27	3.5	Long Wave	0.40

B. Optimal Voyage Scheduling of AES

After obtaining the optimal sea route of AES, the voyage scheduling is performed to minimize the total operation cost of AES, which mainly includes the generation costs of DSG and ESS. This is achieved through the hourly speed adjustment and energy management of AES. Take a single (the k^{th}) AES as an example, the optimization model is formulated as [7]

$$\min_{v_{k,t},P_{DSG,k,t},P_{dis,k,t}} C_k = \sum_{t=T_{s,k}}^{T_{a,k}} (C_{ESS,k,t} + C_{DSG,k,t}) \tag{3}$$

$$C_{DSG,k,t} = c_2 P_{DSG,k,t}^2 + c_1 P_{DSG,k,t} + c_0 \tag{4}$$

$$\begin{cases} C_{ESS,k,t} = \dfrac{TC_{ESS,k} P_{dis,k,t} \Delta t}{2 L_{ESS,k,t} E_{ESS,k,t} D_{ESS,k,t} \eta_{ch} \eta_{dis}} \\ L_{ESS,k,t} = \alpha_0 D_{ESS,k,t}^{\alpha_1} e^{\alpha_2 D_{ESS,k,t}} \\ D_{ESS,k,t} = \dfrac{P_{dis,k,t} \Delta t}{E_{ESS,k}} \end{cases} \tag{5}$$

$$P_{DSG,k,t} + P_{dis,k,t} = P_{pl,k,t} + P_{sv1,k,t} \tag{6}$$

$$P_{pl,k,t} = \rho_1 (1 + f_t)(v_{k,t})^{\rho_2} \tag{7}$$

$$\begin{cases} P_{DSG,k}^{min} \leq P_{DSG,k,t} \leq P_{DSG,k}^{max} \\ \left| P_{DSG,k,t+1} - P_{DSG,k,t} \right| \leq P_{DSG,k}^{ramp} \end{cases} \tag{8}$$

$$\begin{cases} P_{\mathrm{dis},k}^{\min} \le P_{\mathrm{dis},k,t} \le P_{\mathrm{dis},k}^{\max} \\ SOC_{k,t} = SOC_{k,t-1} + P_{\mathrm{dis},k,t}\Delta t / (\eta_{\mathrm{dis}} E_{\mathrm{ESS},k}) \\ SOC^{\min} \le SOC_{k,t} \le SOC^{\max} \end{cases} \tag{9}$$

$$\begin{cases} v_{k,t}^{\min} \le v_{k,t} \le v_{k,t}^{\max} \\ \sum_{t=T_{s,k}}^{T_{a,k}} v_{k,t}\Delta t = d_{\mathrm{route}} \end{cases} \tag{10}$$

The main objective considered for voyage scheduling is illustrated in (3). It includes the DSG fuel consumption cost in (4) and battery degradation cost in (5) for all cruising periods. Specifically, $C_{\mathrm{DSG},k,t}$ is expressed as a quadratic function of $P_{\mathrm{DSG},k.t}$, while $C_{\mathrm{ESS},k,t}$ is formulated based on the depth of discharge (DOD) and battery lifetime functions [26]. Equation (6) is the active power balance constraint, where the power generation of DSG and ESS should meet the requirements of AES's propulsion power and service load. The propulsion power is then formulated in (7) as a function of vessel speed and sea resistance. Note that f_t is estimated based on f_{ij} along the sea route and assumed to be known once route planning is completed. Equation (8) represents the power generation and ramp rate constraints of DSG. Equation (9) describes the discharging power and SOC constraints of ESS. Since ESS is responsible for supporting loads on AES, only the discharge process is considered during the voyage scheduling. Equation (10) denotes that the vessel speed is bounded to ensure safety and should satisfy the functional relationship between total route distance and cruising time periods.

It is admitted that wind speed and wave height are all uncertainty variables, and their time-varying characteristics may cause inaccuracy in sea resistance estimation. To address this issue, the voyage scheduling problem can be extended to a robust optimization model against uncertainties. Specifically, sea resistance f_t in (7) is converted to an uncertainty variable within the box uncertainty set, while objective function (3) is modified to a "max-min" problem that also maximizes C_k over f_t. Detailed modeling and solution methods of robust optimization are presented in [10], [28] for interested readers.

IV. Voltage Regulation in Seaport Microgrids with Berth Allocation

A. Volt/Var Optimization in Microgrids

Different from voltage regulation in land-based microgrids, the volt/var optimization in seaport microgrids must consider the charging power of AES at the port bus. To minimize total power losses while mitigating voltage violations, the optimization model is formulated as

$$\min_{tap_t, Q_{\mathrm{PV}i,t}} \sum_{t\in T}\sum_{ij\in E} \frac{P_{ij,t}^2 + Q_{ij,t}^2}{V_s^2} r_{ij} \tag{11}$$

$$\begin{cases} P_{\mathrm{PV},j,t} - P_{\mathrm{S},j,t} - P_{\mathrm{L},j,t} = \sum_{jk\in E} P_{jk,t} - \sum_{ij\in E} P_{ij,t} \\ Q_{\mathrm{PV},j,t} - Q_{\mathrm{L},j,t} = \sum_{jk\in E} Q_{jk,t} - \sum_{ij\in E} Q_{ij,t} \end{cases} \tag{12}$$

$$V_{i,t} = V_{j,t} + \frac{P_{ij,t} r_{ij} + Q_{ij,t} x_{ij}}{V_s} \tag{13}$$

$$\begin{cases} V^{\min} \le V_{i,t} \le V^{\max} \\ V_{1,t} = V_s + tap_t \cdot \Delta V_{\mathrm{T}} \end{cases} \tag{14}$$

$$\sum_{t=1}^{T} \left| tap_{t+1} - tap_t \right| \le tap^{\max} \tag{15}$$

$$\left| Q_{\mathrm{PV},i,t} \right| \le \sqrt{S_{\mathrm{PV}}^2 - P_{\mathrm{PV},i,t}^2} \tag{16}$$

where equation (11) is the objective function aiming at minimizing total active power losses along all branches for all time periods. Equations (12)-(13) are the linearized distribution load flow model, which describes the active, reactive power flow and voltage relationship constraints respectively. Considering its relatively high computing efficiency and accuracy, the linearized distribution load flow model has been widely used in voltage control problems in distribution networks [27]. In Equation (14), the first sub-equation is the upper and lower voltage limits while the second sub-equation is the substation voltage with the OLTC position. The daily switching times of OLTC are constrained in (15) to extend the lifetime and the reactive power capability of inverter-based PVs is shown in (16). Since voltage violations can occur in microgrids due to the heavy charging demand of AES, voltage constraints (14) are formulated to ensure voltage security. It is worth noting that network thermal limits are also of importance to achieve the secure operation of seaport microgrids. The optimization model can be extended to incorporate thermal limits by adding constraints on branch power flows as $P_{ij,t}^2 + Q_{ij,t}^2 \le (S_{ij}^{\max})^2$, where $S_{ij}^{\max}$ is the maximum power flow on branch ij.

B. Proposed Extended OPF with Berth Allocation

In practice, when the AES arrives at the seaport, it will be assigned to a berth and receive charging services from the microgrid. On the one hand, the microgrid provides active power to charge ESS on AES; on the other hand, the grid supplies electrical power to EPC for cargo handling. Therefore, the total charging power injection to the seaport is formulated in (17).

$$P_{\mathrm{S},j,t} = \sum_{m\in B}\sum_{k\in A} \omega_{m,k,t} (P_{\mathrm{ch},m,k,t} + P_{\mathrm{EPC},m,t} + P_{\mathrm{sv2},k,t}) \tag{17}$$

where $P_{EPC,m,t}$ is the constant charging power for EPC at time t and only varies with different berths; $P_{\mathrm{sv2},k,t}$ is the constant service load of the k^{th} berthed-in AES at time t. The value of $P_{\mathrm{ch},m,k,t}$ is determined by the arrival SOC, arrival time and berthing time at the seaport, which can be calculated in (18).

$$P_{\mathrm{ch},m,k,t} = \frac{(SOC_f - SOC_{a,k}) E_{\mathrm{ESS},k}}{\eta_{\mathrm{ch},k} \delta_{m,k}} \tag{18}$$

where SOC_f is the required SOC when AES leaves the seaport and equals to $SOC^{\max}$; $\delta_{m,k}$ is the predefined berthing time of the k^{th} AES at the m^{th} berth, which is usually consistent with the cargo handling time at a specific berth. The AES should also satisfy the following constraints to calculate $\omega_{m,k,t}$ in the berth allocation problem.

$$\sum_{k\in A} \omega_{m,k,t} \le 1, \ \sum_{m\in B} \omega_{m,k,t} \le 1 \tag{19}$$

$$\begin{cases} T_{b,k} + \sum_{m\in B}\sum_{t\in T} \omega_{m,k,t} = T_{f,k} \\ T_{b,k} \ge T_{a,k} \end{cases} \tag{20}$$

$$\begin{cases} t\omega_{m,k,t} + (1-\omega_{m,k,t})M \geq T_{b,k} \\ (t+1)\omega_{m,k,t} \leq T_{f,k} \end{cases} \tag{21}$$

$$\sum_{m\in B}\sum_{k\in A}\mu_{m,k,t} = 1,\ \sum_{k\in A}\mu_{m,k,t} \leq 1 \tag{22}$$

$$T_{b,k} = \sum_{m\in B}\sum_{t\in T} t\mu_{m,k,t} \tag{23}$$

$$\sum_{m\in B}\sum_{t\in T}\mu_{m,k,t}\delta_{m,k} = T_{f,k} - T_{b,k} \tag{24}$$

$$\sum_{t\in T}\omega_{m,k,t} \leq \sum_{t\in T} t\mu_{m,k,t} \tag{25}$$

where equation (19) enforces that each berth can only serve at most one vessel, and each vessel can only be assigned to one berth at a time. Equation (20) describes the relationship between vessel arrival time, service start time and completion time. Equation (21) ensures that the berthing time of a vessel should be in the range between service start and completion times. Equation (22) means that the vessel can only start service at one berth at a time while equation (23) formulates the relationship between T_{bk} and $\mu_{m,k,t}$. Equation (24) enforces that the total service time of a vessel is equal to the predefined berthing time. Equation (25) states that a vessel cannot change the berth position during the charging service process.

To sum up, the extended voltage regulation model in seaport microgrids is formulated as below.

$$\min_{tap_t, Q_{\mathrm{PV}i,t}, \omega_{m,k,t}} \sum_{t\in T}\sum_{ij\in E}\frac{P_{ij,t}^2 + Q_{ij,t}^2}{V_s^2} r_{ij} \tag{26}$$

$$\text{s.t.} \quad (12)-(25) \tag{27}$$

Compared with coordinated energy management and berth allocation models [20]-[24], our model makes an improvement in two aspects: (1) We introduce integer variables $T_{a,k}$, binary variables $\mu_{m,k,t}$ and additional constraints (22)-(25), so that the model can flexibly regulate arrival times of AES at different berths to improve the voltage regulation performance. (2) We assume that AES and microgrid operators are in a cooperation mode, where berth allocation problems are directly integrated into volt/var optimization to improve voltage profiles. The berthing times only satisfy time constraints (19)-(25) and will not be minimized in [21], [22]. The proposed optimal voltage regulation model can also be extended to address the uncertainty issues of PVs with stochastic or robust optimization methods.

V. Solution Methodology

A. Proposed T_a-SOC_a Pairs and Satisfactory Index

This section introduces the proposed T_a-SOC_a pairs that help design the coordinated voltage regulation and voyage scheduling strategy. Here, the idea is to simultaneously adjust the arrival time, arrival SOC and service berth of AES to achieve secure and optimal operation in seaport microgrids. The arrival time of an AES is subject to a certain range with an hour resolution and is formulated as below.

$$T_{a,k} \in [T_{a,k}^{\mathrm{low}}, T_{a,k}^{\mathrm{up}}] \cap Z_+ \tag{28}$$

where $T_{a,k}^{\mathrm{low}}$ and $T_{a,k}^{\mathrm{up}}$ are the earliest and latest arrival times of the k^{th} AES; Z_+ denotes the nonnegative integer set. The $SOC_{a,k}$ is obtained by repeatedly solving the optimization problem (3)-(10) under each $T_{a,k}$ and is formulated in (29).

$$SOC_{a,k} = SOC_{k,t|t=T_{a,k}} = \{\arg\min C_k \mid \text{s.t. } (4)-(10)\} \tag{29}$$

where C_k is the total operation cost of the k^{th} AES expressed in (3). The $T_{a,k}$ and $SOC_{a,k}$ will formulate multiple T_a-SOC_a pairs and have strict one-to-one correspondence. Moreover, a customized SI is designed to ensure the operation cost is acceptable to each AES. For a specific $T_{a,k}$, the value of SI is then calculated in (30).

$$\mathrm{SI}_k = \frac{C_k^{\max} - C_k}{C_k^{\max} - C_k^{\min}} \tag{30}$$

where $C_k^{\max}$ and $C_k^{\min}$ are the maximum and minimum operation costs of AES considering all T_a-SOC_a pairs. For each vessel, SI_k is in the range [0,1] and should be larger than a customized threshold β_k to maintain a higher satisfaction. If $\mathrm{SI}_k<\beta_k$ is satisfied, the corresponding T_a-SOC_a pair will be discarded due to an unacceptable C_k of AES users.

B. Model Reformulation and Linearization

By applying the condition $\mathrm{SI}_k \geq \beta_k$, several T_a-SOC_a pairs with lower operation costs are selected for the voltage regulation problem. Therefore, the functional relationship between $T_{a,k}$ and $SOC_{a,k}$ should be formulated and added as constraints in the optimization model (26)-(27). In this paper, such a relationship is established based on piecewise linear functions and expressed as below.

$$\begin{cases} SOC_{a,k} = \sum_{j=1}^{N_{pk}} (a_{k,j}T_{a,k,j} + b_{k,j}\lambda_{k,j}) \\ T_{a,k,j}^{p}\lambda_{k,j} \leq T_{a,k,j} \leq T_{a,k,j+1}^{p}\lambda_{k,j} \\ T_{a,k} = \sum_{j=1}^{N_{p,k}} T_{a,k,j} \\ \sum_{j=1}^{N_{p,k}} \lambda_{k,j} = 1 \end{cases} \tag{31}$$

where $a_{k,j}$ and $b_{k,j}$ are the slope and y-axis intercept for jth piecewise linear function and can be calculated based on T_a-SOC_a pairs; $T_{a,k,j}^{p}$ is the endpoint value of discrete vessel arrival times; $\lambda_{k,j}$ is a binary variable indicating the k^{th} piecewise function; $N_{p,k}$ is the total number of piecewise functions.

In this work, nonlinear constraints in both voyage scheduling and voltage regulation optimization problems are further reformulated as linear functions to achieve effective solutions. Specifically, the nonlinear battery lifetime function in equation (5) and propulsion power function in equation (7) can be linearized with the same piecewise linear function illustrated in (31) [7]. The nonlinear absolute terms in constraints (8) and (15) are then equivalently converted to (32) and (33) respectively.

$$\begin{cases} P_{\mathrm{DSG},k,t+1} - P_{\mathrm{DSG},k,t} \leq P_{\mathrm{DSG},k}^{\mathrm{ramp}} \\ P_{\mathrm{DSG},k,t} - P_{\mathrm{DSG},k,t+1} \leq P_{\mathrm{DSG},k}^{\mathrm{ramp}} \end{cases} \tag{32}$$

$$\begin{cases} tap_{t+1} - tap_t \leq \gamma_t \\ tap_t - tap_{t+1} \leq \gamma_t \\ \sum_{t=1}^{T}\gamma_t \leq tap^{\max} \end{cases} \tag{33}$$

where γ_t is an auxiliary integer variable indicating the tap change of OLTC from time t to t+1. Moreover, the product of

$\omega_{m,k,t}$ and $P_{\mathrm{ch},m,k,t}$ in equation (17) also brings nonlinearity to the model. Let $x_{m,k,t}=\omega_{m,k,t}P_{\mathrm{ch},m,k,t}$, the following constraint (34) can be added to linearize the original formulation.

$$\begin{cases} x_{m,k,t} \le P_{\mathrm{ch},m,k,t} \\ x_{m,k,t} \ge P_{\mathrm{ch}m,k,t} - M(1-\omega_{m,k,t}) \\ P^{\mathrm{low}}_{\mathrm{ch},m,k,t}\omega_{m,k,t} \le x_{m,k,t} \le P^{\mathrm{up}}_{\mathrm{ch},m,k,t}\omega_{m,k,t} \end{cases} \tag{34}$$

where $P^{\mathrm{low}}_{\mathrm{ch},m,k,t}$ and $P^{\mathrm{up}}_{\mathrm{ch},m,k,t}$ are the lower and upper bounds of $P_{\mathrm{ch},m,k,t}$. They are parameters for the optimization problem and can be calculated in advance based on T_a-SOC_a pairs and equation (18). In equations (31)-(34), all linearization points are fixed, while they might also be updated based on newer solutions to further improve the accuracy of the linearization process. To this end, both the reformulated optimal voyage scheduling and voltage regulation problems are mixed-integer quadratic programs (MIQP) that can be effectively solved with commercial solvers.

C. Customized Coordinated Optimization Procedure

After model reformulation and linearization, we can finally obtain two key optimization models for achieving the coordination between voyage scheduling and voltage regulation. The first one is the optimal voyage scheduling model of AES, which is formulated as {(3)-(10), (32)} with decision variables $v_{k,t}$, $P_{\mathrm{DSG},k,t}$ and $P_{\mathrm{dis},k,t}$. The second one is the optimal voltage regulation model of seaport microgrids, which is formulated as {(26)-(27), (31), (33)-(34)} with decision variables tap_t, $Q_{\mathrm{PV}i,t}$, $\omega_{m,k,t}$, $\mu_{m,k,t}$, $T_{ak,j}$ and $\lambda_{k,j}$. Although the two optimization problems are linearized to MILP for efficient solutions, they cannot emerge into one optimization model and be solved simultaneously. This is because AES and microgrids are two separate entities and their objectives may be conflicting, which cannot be simply combined into one objective with weighting factors. Also, the AES and microgrids may not be willing to share information due to privacy concerns. Therefore, the solution process should be conducted in a sequential and distributed manner with limited information exchange.

To balance the benefits between AES and microgrid operators, a customized coordinated optimization procedure is developed. This method first repeatedly solves the voyage scheduling problem under each possible T_a to obtain multiple T_a-SOC_a pairs. Then, the SI is calculated for each vessel and only T_a-SOC_a pairs satisfying $\mathrm{SI}_k \geqslant \beta_k$ are reserved. Finally, the optimal voltage regulation is performed to find the best T_a-SOC_a pair and achieve optimal operation in microgrids. The "customized" means each vessel can define an individual threshold to satisfy the minimum SI and result in an acceptable operation cost. Thus, by carefully selecting the T_a-SOC_a pairs, the operation cost of AES is reduced while the power losses of microgrids are also minimized within secure voltage ranges, achieving the coordination between voyage scheduling and voltage regulation. The detailed process of the coordinated optimization method is shown below.

Algorithm 1 Customized Coordinated Optimization Procedure

1: Initialization: Initialize sea conditions, PV and load prediction in microgrids, berth number and EPC power at the seaport, and basic settings of each AES.

2: Solve the optimal route planning model: Solve the optimization problem (1)-(2) with added resistance, and obtain an optimal sea route with the distance d_{route}.

3: Solve the optimal voyage scheduling model: Repeatedly solve the optimization problem {(3)-(10), (32)} under each T_a, obtain multiple T_a-SOC_a pairs along with $v_{k,t}$, $P_{\mathrm{DSG},k,t}$ and $P_{\mathrm{dis},k,t}$ for all AES.

4: Selection of T_a-SOC_a pairs: The AES calculates SI based on (30), defines an individual threshold β_k and only reserves T_a-SOC_a pairs satisfying $\mathrm{SI}_k \geqslant \beta_k$.

5: Solve the optimal voltage regulation model with berth allocation: Solve the optimization problem {(26)-(27), (31), (33)-(34)}, obtain the optimal $T_{a,k}$-$SOC_{a,k}$ pairs and dispatch results tap_t, $Q_{\mathrm{PV}i,t}$ and $\omega_{m,k,t}$.

6: Determine the voyage scheduling strategy: Based on $T_{a,k}$ derived in Step 5 and dispatch results obtained in Step 3, determine the corresponding optimal voyage scheduling strategy for each vessel.

VI. Case Study

The simulations were conducted using MATLAB® on a 64-bit laptop with 2.60 GHz CPU and 16GB RAM. The MIQP optimization models were programmed on GAMS and solved by the CPLEX solver.

A. Test System and Parameters Settings

In this paper, the vessel sails from the start port to the seaport microgrid and berths at the seaport to receive charging and cargo handling services. Based on (1)-(2), an optimal sea route is first determined with a total distance d_{route} of 30 nautical miles. All vessels start cruising at 8:00, arrive at the seaport between $T^{\mathrm{low}}_{a,k}$=10:00 and $T^{\mathrm{up}}_{a,k}$=12:00, and finally leave the port before 17:00. For $T_{a,k}$=10:00, 11:00 and 12:00, the values of hourly added resistance f_t are estimated as [0.17,0.2], [0.18,0.24,0.15] and [0.15,0.2,0.3,0.1] respectively. In the voyage scheduling phase, the proposed method is applied to four different AES, where detailed parameters of DSG, ESS and service load are presented in Table II. The vessel speed is bounded within $[v_t^{\min},v_t^{\max}]$=[5,20] knots. The parameters ρ_1 and ρ_2 for the propulsion power are 0.0355 and 3.165 respectively. The generation cost coefficients of DSG (c_0,c_1,c_2) take the values of (3.02e-5,0.37,0.01). The ESS has an investment cost $TC_{\mathrm{ESS},k}$ of $ 600 per kW, while the coefficients of battery lifetime function (α_0,α_1,α_2) are (1.69e4,-0.24,-2.57) [26]. Here, $TC_{\mathrm{ESS},k}$ refers to the life cycle cost of ESS including acquisition cost, installation cost, daily maintenance cost, etc., which is predefined and used to calculate $C_{\mathrm{ESS},k,t}$ based on (5). The battery SOC is operating in the range $[SOC^{\min},SOC^{\max}]$=[0.1,0.9] with the charging/discharging efficiencies $\eta_{\mathrm{ch}}/\eta_{\mathrm{dis}}$ at 95%.

In the voltage regulation phase, our method is verified on a modified EU 16-bus seaport microgrid based on [29], where detailed network topology and system parameters are provided in Appendix. The microgrid operates in grid-connected mode and consists of one OLTC, four PVs and one seaport. The OLTC is located at bus 1 and has 20 taps with a ΔV_{T}=0.005 p.u and V_s=1.0 p.u. The PVs 1-4 have the same capacity of 100 kW and are located at buses 4, 7, 14 and 16 respectively.

Fig. 2 presents the day-ahead hourly prediction of PV and load curves in the microgrid. As practical microgrids are usually small-scale networks, all four PVs located in this area are assumed to share the same generation curve. The loads are also assumed to have the same load type (residential) and share one load curve. The P_{PV}^{max} represents rated PV generation and equals 100 kW, while P_{L}^{max} and Q_{L}^{max} are rated active and reactive loads presented in Table A1 in Appendix. In addition, PVs are assumed to be owned and controlled by the microgrid operator. They produce electricity and sell it to customers (load) in microgrids, while the microgrid buys electricity from the upper grid. The microgrid may also sell electricity to the upper grid if there is a surplus in PV generation after balancing load demand. Commonly, the voltage regulation emphasizes the interaction and balance of power, where the financial transactions in energy trading are not considered. The seaport is located at bus 15 with three berths and corresponding EPC. The detailed parameters of EPC power, cargo handling time, and service loads for berthed-in AES are listed in Table III. The term "AES 2 (3)" means AES 2 and AES 3 are of the same vessel type and thus have the same berthing time, which is common in practical seaport operation. The security voltage operating range $[V^{min},V^{max}]$ is equal to [0.95,1.05] p.u. and the threshold β_k is set as 0.5 for all AES.

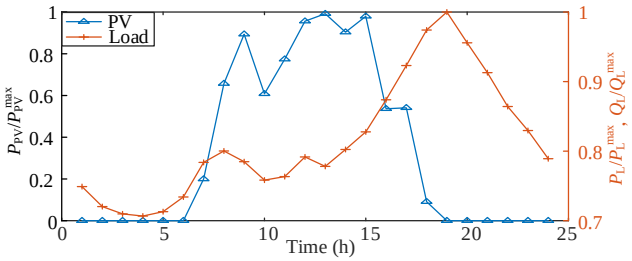

Fig.2. Day-ahead hourly prediction of PV and load curves in the microgrid

Table II. Detailed parameters of DSG and ESS on four AES

Vessels	Types	Device	P^{max} (kW)	P^{min} (kW)	P^{ramp}/E_{ESS} (kW)	P_{sv1} (kW)
AES 1	1	DSG	300	80	200	10
		ESS	60	10	120	
AES2 (3)	2	DSG	400	120	200	20
		ESS	90	10	180	
AES 4	3	DSG	500	170	300	30
		ESS	120	10	240	

Table III. Detailed parameters for EPC and AES at berths

Berths	P_{EPCm}	P_{sv2} (kW) for AES 1-4	$\delta_{m,k}$ (hour)		
			AES 1	AES 2 (3)	AES 4
Berth 1	15	[10,20,20,30]	2	4	6
Berth 2	15		2	4	6
Berth 3	30		1	2	3

B. Analysis of T_a-SOC_a Pairs and Selection of β_k

Before making a comprehensive comparison study, this section provides a detailed analysis of T_a-SOC_a pairs and β_k of the proposed method. Fig. 3 presents the proposed T_a-SOC_a pairs for four AES along with SI values denoted on each bar. It is observed that the arrival SOC has an increasing trend with the arrival times of AES. The highest SI occurs at T_a=11 for all vessels, while several T_a-SOC_a pairs with SI<0.5 are discarded (blank bar). This also illustrates that the shortest cruising time (T_a=10) in voyage scheduling cannot lead to the lowest operation cost, and the schedule of arrival times with SI is necessary to ensure the benefits of AES. Fig. 4 shows the sensitivity analysis of acceptable vessel arrival times T_a to the threshold β_k. When β_k is equal to zero, the operation cost in voyage scheduling is not constrained and all T_a-SOC_a pairs can be reserved for voltage regulation. As the increase of β_k, some T_a-SOC_a pairs with higher operation costs are limited and the number of acceptable T_a is decreasing. In practice, the value of β_k can be negotiated by both AES users and microgrid operators to achieve a win-win situation. Specifically, when AES users benefit from lower operation costs (larger values of β_k), the microgrids will make compromises that may result in higher power losses and voltage violation risks, and vice versa. Therefore, a win-win situation means that under the premise of voltage security, the operation cost and power losses are partially reduced and accepted by AES and microgrids respectively.

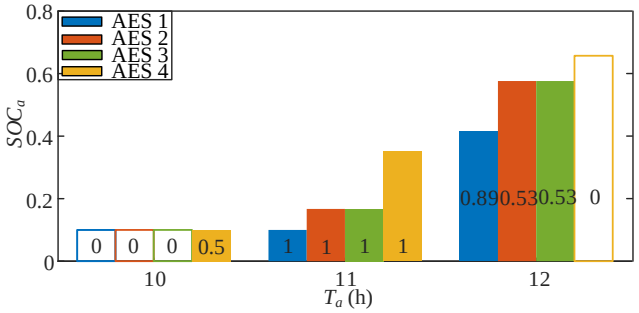

Fig. 3. T_a-SOC_a pairs and corresponding SI values for all AES

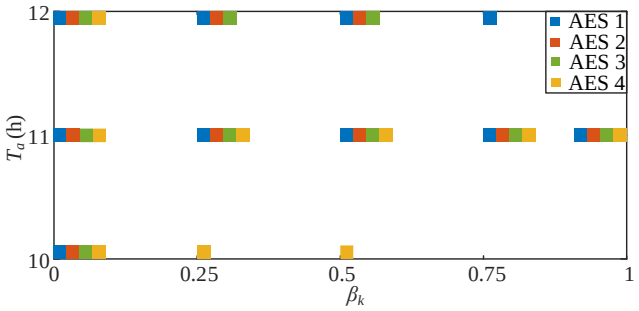

Fig.4. Sensitivity analysis of acceptable vessel arrival times to β_k

C. Numerical Comparison Results of Voyage Scheduling and Voltage Regulation

To demonstrate the advantages of the proposed coordinated optimization method, three existing voyage scheduling and voltage regulation strategies are evaluated and described as below.

Method #1: Optimal voyage scheduling. This method first solves voyage scheduling problems to find the optimal T_a-SOC_a pairs that can minimize the operation cost of each AES. Based on predefined T_a-SOC_a pairs ($T_{a,k}$=11), the MGCC solves the extended voltage regulation problem to achieve optimal operation in seaport microgrids. Therefore, Method #1 can minimize the operation cost during voyage scheduling but fails to mitigate the potential negative impacts on voltage regulation in microgrids. Similar methods that only focus on optimal voyage scheduling can be found in [7], [11].

Method #2: Optimal voltage regulation with adjustable SOC_a range. This approach aims to achieve optimal operation in seaport microgrids by flexibly adjusting $SOC_{a,k}$, which is at

the expense of increasing the operation cost of AES. Different from (31) in our method, $SOC_{a,k}$ is independent of $T_{a,k}$ and can be adjusted within a range [0.1,0.6]. The MGCC solves the voltage regulation problem to obtain $T_{a,k}$ and $SOC_{a,k}$, which are then substituted into the voyage scheduling problem to update the generation scheduling results. This method represents theoretically the optimal voltage control performance in microgrids and is only developed for comparison purposes.

Method #3: Optimal voltage regulation with minimum service time. Considering the scenario that AES users are sensitive to waiting and cargo handling times, the method achieves optimal voltage regulation while minimizing the total service time of vessels [20], [22]. This is achieved by adding another term $\sum(T_{f,k}\text{-}T_{a,k})$ to the objective function (26), and other control strategies are the same as the proposed method.

Fig. 5 presents the velocity of AES during the voyage scheduling under different methods. In Method #1, all AES sails to the seaport with a constant velocity of 10 knots in 3 hours, which balances the propulsion power and cruising time to reduce total operation cost. In Method #2, AES 1-3 sail at a constant velocity of 10 knots while AES 4 adopts a much higher velocity of 15 knots. This is because the T_a of AES 4 is adjusted to 10:00 and it must increase the cruising speed to arrive at the seaport on time. By contrast, in Method #3 and the proposed method, AES 1 and AES 3 keep a lower velocity of about 7 knots due to a relatively longer cruising time of 4 hours. Fig. 6 then illustrates the generation scheduling results of DSG and ESS on AES during the voyage scheduling under different methods. Since the per-unit cost of ESS is usually lower than that of DSG, Method #1 leads to more ESS discharging power and less DSG generation to balance loads compared with other methods. However, Method #2 mainly focuses on reducing power losses in microgrids and causes the highest DSG generation for all AES. The generation scheduling of Method #3 and the proposed method are almost the same and their DSG generation remains at a middle level between Method #1 and Method #2. Considering the largest DSG/ESS capacity and earliest arrival times, AES 4 also results in the highest generation power compared with other vessels.

Fig. 7 shows the berth allocation results of AES at the seaport under different methods. In Method #1, with the uniform arrival times of 11:00, the berthing times of AES are centered around 12:00 and cause heavy load demand in this period. Method #2 assigns AES 2 to berth 1 and other AES to berth 3 respectively, which evenly distributes the charging demand to each period between 10:00 and 15:00. To minimize the total service time in voltage regulation, Method #3 fully utilizes all three berths to simultaneously provide charging and cargo handling services for AES. The proposed method adopts a berth allocation strategy similar to Method #2, where the difference in the service sequence of AES 1-3 is caused by the varying arrival times and charging power.

Fig. 8 shows the voltage profiles in seaport microgrids under different methods. In Fig. 8(a), all bus voltages are controlled to the security operating levels with the proposed method, and the minimum voltage occurs at 12:00 and 14:00 even with high PV generation. In Fig. 8(b), the minimum voltage at bus 15 suddenly drops at 10:00 due to the increased charging demand of berthed-in AES. During the AES berthing time between 10:00 and 15:00, the minimum voltages for all methods approach the lower limits and fluctuate within [0.95,0.98] p.u. The voltages are maintained in security ranges through the coordinated control of OLTC, PV and AES. Fig. 9 presents the hourly dispatch of these devices in seaport microgrids under different methods, including OLTC's tap position in Fig. 9(a), PV4's reactive power in Fig. 9(b) and AES's charging power in Fig. 9(c) respectively. The OLTC must be tapped up in Method #1 and Method #3 to address voltage problems, but it is tapped down in Method #2 and the proposed method to achieve a flat voltage profile and reduce power losses. In terms of the reactive power of PV4, Method #1 also needs to provide an extra 14.3kVar reactive power to mitigate voltage violations at 12:00 compared with our method. By adjusting $SOC_{a,k}$ to a higher level (e.g., SOC_{a4}=0.6), Method #2 leads to the lowest charging power of AES during most berthing periods. The average AES charging power of the proposed method is reduced to 150 kW to help reduce power losses, while it still remains at a middle level between Method #1 and Method #2.

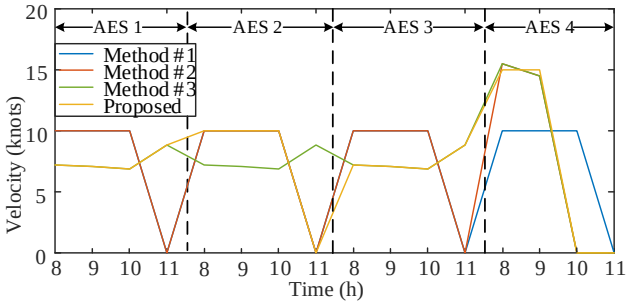

Fig.5. Velocity of AES during the voyage scheduling under different methods

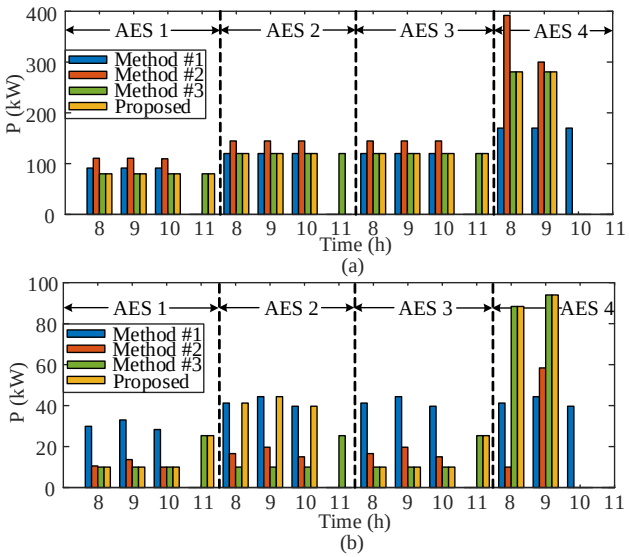

Fig.6. Generation scheduling of AES during the voyage scheduling under different methods: (a) DSGs, (b) ESS

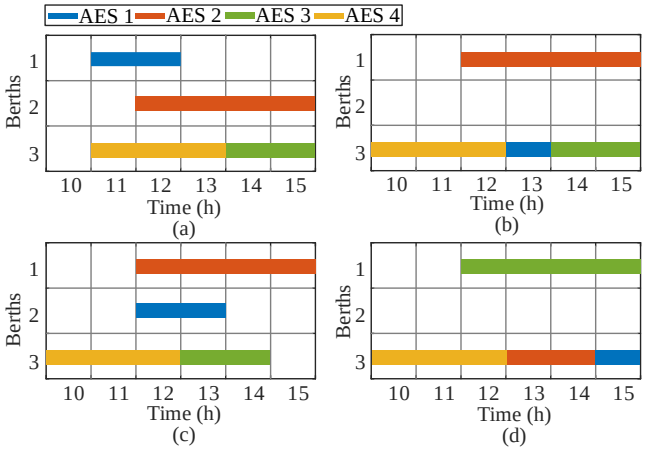

Fig. 7. Berth allocation results of four AES under different methods: (a) Method #1, (b) Method #2, (c) Method #3, (d) Proposed method

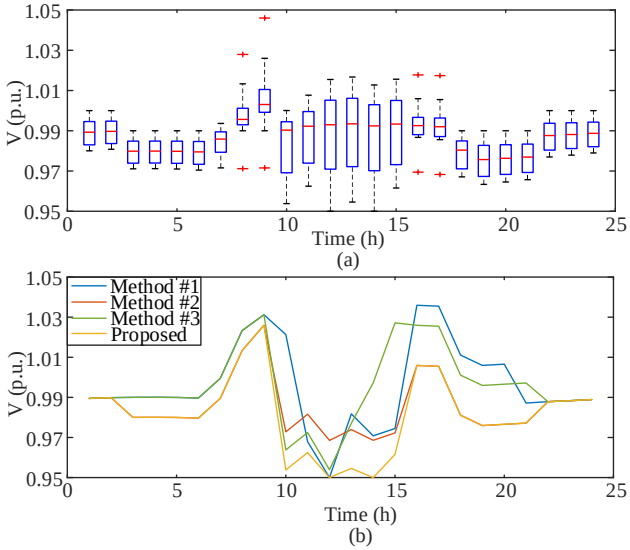

Fig. 8. Voltage profiles in seaport microgrids under different methods: (a) Voltage of all buses with the proposed method, (b) Minimum voltage at bus 15 under different methods

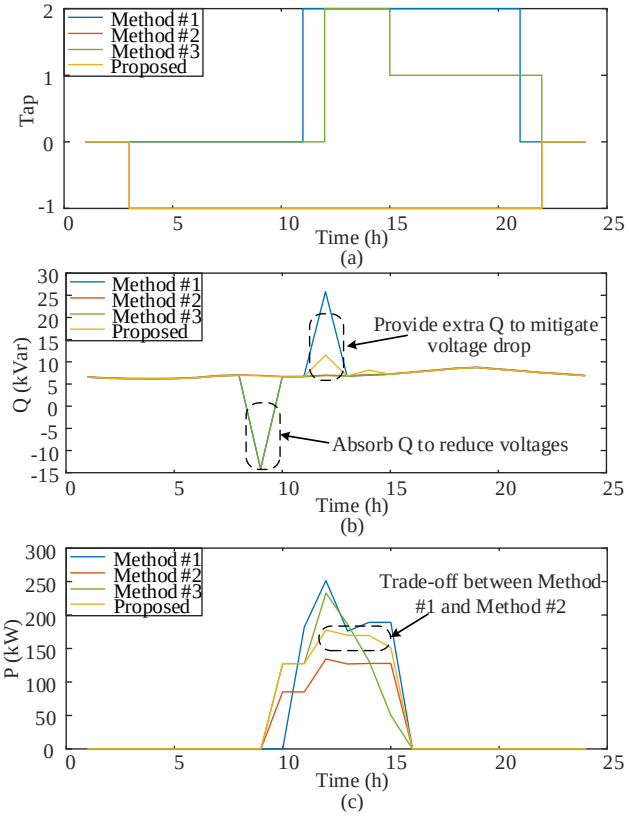

Fig. 9. Dispatch of OLTC, PVs and AES in seaport microgrids under different methods: (a) OLTC, (b) Reactive power of PV 4, (c) Charging power of AES

Table IV. Numerical voyage scheduling and voltage regulation comparison results under different methods

Methods	Operation cost ($)	Power losses (kWh)	AES waiting time (h)	AES berthing time (h)
Method #1	613.88	136.41	4	11
Method #2	730.75	108.12	6	10
Method #3	724.84	124.43	1	11
Proposed	688.10	120.00	5	10

Finally, the numerical comparison results of voyage scheduling and voltage regulation under different methods are summarized in Table IV. Method #1 only aims at optimizing the voyage scheduling process, which results in the lowest operation cost of $613.88 and the highest power loss of 136.41 kWh in microgrids. Similarly, Method #2 has the lowest power losses and the highest operation cost compared with other methods. The SI values for some vessels in Method #2 even violate the threshold β_k and cannot be accepted by AES users. By contrast, our method leads to a 12.03% power loss reduction compared to Method #1 and a 5.8% operation cost reduction compared to Method #2 respectively. To this end, the proposed method successfully finds a trade-off between reducing operation costs and power losses to achieve a win-win situation. In addition, Method #3 is designed especially for AES users who are sensitive to time consumption. This method can minimize the AES service time to 12 hours, which includes 1 hour waiting time and 11 hours berthing time. However, this is also at the expense of an extra $ 36.74 operation cost and 4.43 kWh power losses compared with the proposed method.

D. Discussion

(1) Rationale of the bi-objective optimization process

The primary motivation for using a bi-objective optimization process is that microgrid operators and AES users are two independent entities with different interests and objectives. They will not share data in uncooperating modes, and such an optimization process preserves privacy with limited information exchange. Although the cost of power losses of microgrids is much smaller than the operation cost of AES, the cost saving of AES cannot be used to compensate for economic losses of microgrids. Moreover, for larger-scale seaport distribution networks, the cost of power losses is considerable and may even exceed AES's operation cost. In this case, simulations are then conducted on a modified IEEE 33-bus distribution network [30]. In the test system, there are six PVs located at buses 4, 12, 16, 25, 30 and 33, while other parameters are the same as those in the microgrid. Table V compares voltage control results under different methods in seaport distribution networks and similar conclusions are found. The proposed method still successfully balances benefits between AES users and microgrid operators, verifying the scalability in large-scale networks. Notably, with an average electricity price of $ 0.5/kWh, the cost of network power losses exceeds $ 850 and becomes higher than the operation costs of AES. This illustrates the rationale of the bi-objective optimization process in practical implementation.

Table V. Comparison of voyage scheduling and voltage regulation results under different methods in modified IEEE 33-bus distribution networks

Methods	Operation cost ($)	Power losses (kWh)	AES waiting time (h)	AES berthing time (h)
Method #1	613.88	1726.21	4	16
Method #2	695.48	1701.45	7	17
Method #3	710.02	1713.26	0	13
Proposed	641.28	1707.22	7	17

(2) Accuracy of linearized optimization model

The linearization of the original optimization problems may introduce errors in the solution process. Based on our simulation results, such errors are relatively small and the linearized model is applicable in practice. For example, the original voyage scheduling problem (3)-(10) can be solved by another nonlinear and nonconvex commercial solver named "OQNLP". It is assumed that this solver obtains global optimal solutions for the formulated small-scale nonconvex optimization problem. Fig. 10 compares the solutions obtained by solving original (nonconvex) and reformulated (proposed) optimal voyage scheduling models of AES 1 in 8:00-9:00 respectively. The relative errors of various variables, such as velocity and operation cost of AES, are quite small (around 2%~4%) and therefore acceptable in practical implementation.

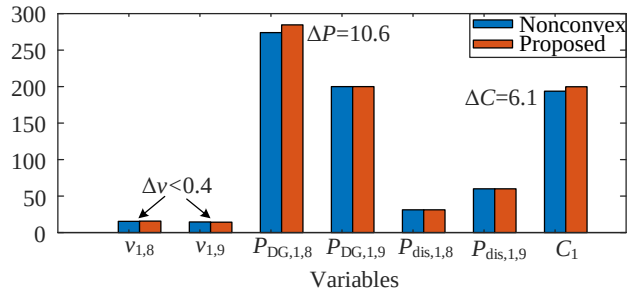

Fig. 10. Comparison of voyage scheduling results of AES 1 in 8:00-9:00 by solving original and reformulated models

(3) Effectiveness in mitigating voltage violations

To verify the effectiveness of the proposed method in mitigating voltage violations, case studies are performed with different arrival times of AES, i.e., between 18:00 and 20:00 in the evening. Due to low PV generation and heavy load demand during this time, the microgrid is more likely to experience voltage drop problems. Fig. 11 presents the berth allocation of AES under different methods in this scenario. The berthing times of AES are postponed to around 22:00, which can shift heavy load in the evening and address voltage drop problems. Fig. 12 shows the corresponding minimum voltages at bus 15 under different methods, where the proposed method still achieves voltage security through coordinated voyage scheduling and berth allocation. However, severe voltage violations are observed in Method #1. This is because optimal voyage scheduling leads to the simultaneous arrival of multiple vessels, which brings heavy charging demand and fails to restore voltages to secure levels even with berth allocation.

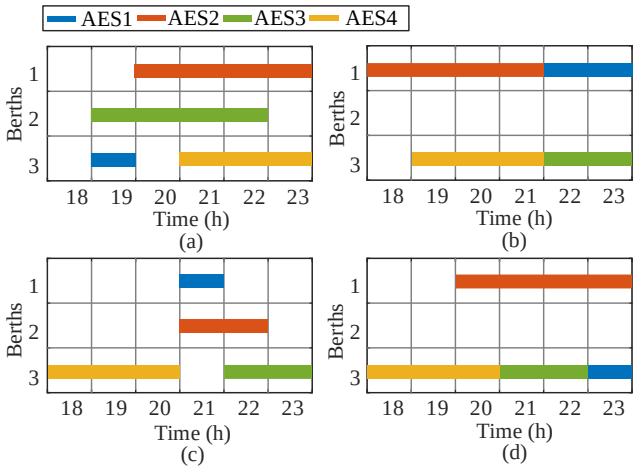

Fig. 11. Berth allocation of AES under different methods with arrival times between 18:00 and 20:00: (a) Method #1, (b) Method #2, (c) Method #3, (d) Proposed method

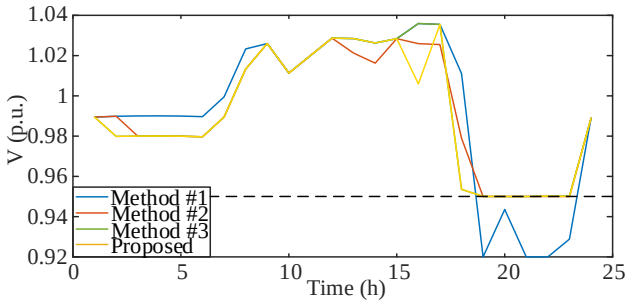

Fig. 12. Minimum voltages at bus 15 under different methods with AES arrival times between 18:00 and 20:00

VII. Conclusion

This paper proposes a customized coordinated voltage regulation and voyage scheduling strategy to regulate voltages in seaport microgrids while balancing the economic benefits between microgrid operators and AES. In this method, the optimal voyage scheduling is performed to dispatch power generation of ESS and DSG and adjust the cruising speed of AES. The extended voltage regulation, incorporating berth allocation and T_a-SOC_a constraints, is then performed to

mitigate voltage violations and reduce power losses through the dispatch of OLTC, PVs and berthed-in AES. The SI is customized for each AES user to ensure an acceptable operation cost during the voyage scheduling. Numerical studies are conducted on a modified EU 16-bus seaport microgrid to obtain the two key conclusions: (1) The proposed method successfully achieves the coordination between voyage scheduling and voltage regulation, which leads to 12.03% power losses reduction and 5.8% operation cost reduction compared to Method #1 and Method #2 respectively. (2) The proposed method can be easily extended to Method #3 to account for the time-sensitive AES users. However, the reduction in total AES service time is at the expense of increased 4.43kWh power losses and $ 36.74 operation cost.

APPENDIX

Fig. A1 presents the one-line diagram of the modified EU 16-bus microgrid with bus numbers, which also illustrates the buses that PVs and the seaport are connected. The detailed line impedance and rated load data are then provided in Table A1. All the data are calculated in per-unit values, where the base power is selected as 400 kVA and the base voltage equals 0.4 kV. The rated line power transmission capacity is assumed to be large enough to host the power of PVs, load and AES as configured. The seaport microgrid is connected to a 20 kV medium voltage distribution grid, where the typical capacity and short circuit power of an external feeder can be 400 kVA and 5.4 MVA respectively.

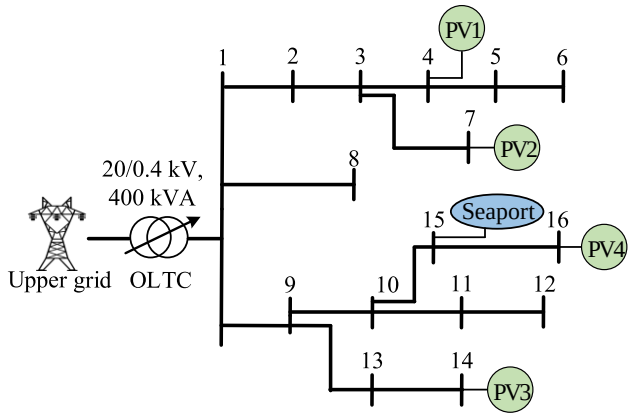

Fig. A1. One-line diagram of the EU 16-bus microgrid

Table A1. Line parameter and rated load demand of the modified EU 16-bus microgrid

From bus i	To bus j	r_{ij} (p.u.)	x_{ij} (p.u.)	Bus number	$P_{L,i}$ (p.u.)	$Q_{L,i}$ (p.u.)
1	2	0.0249	0.00726	1	0	0
1	8	0.132	0.0355	2	0.0128	0.0063
1	9	0.0298	0.0209	3	0	0
2	3	0.0249	0.0073	4	0.0562	0.0275
3	4	0.0497	0.0145	5	0.0128	0.0063
3	7	0.0870	0.0151	6	0.0562	0.0275
4	5	0.0746	0.0218	7	0.1283	0.0627
5	6	0.0249	0.0073	8	0.1575	0.0770
9	10	0.0596	0.0419	9	0.0379	0.0182
9	13	0.0431	0.0221	10	0	0
10	11	0.129	0.0662	11	0.0311	0.0152
10	15	0.0914	0.0239	12	0.0248	0.0121
11	12	0.0431	0.0221	13	0.0311	0.0152
13	14	0.0431	0.0221	14	0.0099	0.0048
15	16	0.0914	0.0239	15	0.0198	0.0097
-	-	-	-	16	0.0099	0.0048

REFERENCES

[1] E. Skjong, R. Volden, E. Rødskar, M. Molinas, T. A. Johansen, and J. Cunningham, "Past, present, and future challenges of the marine vessel's electrical power system," *IEEE Trans. Transp. Elect.*, vol. 2, no. 4, pp. 522–537, Dec. 2016.

[2] D. Kanellos, "Optimal power management with GHG emissions limitation in all-electric ship power systems comprising energy storage systems," *IEEE Trans. Power Syst.*, vol. 29, no. 1, pp. 330-339, Jan. 2014.

[3] E. Sciberras et al., "Electrical characteristics of cold-ironing energy supply for berthed ships," *Transp. Res. D-Transp. Environ*., vol. 39, pp. 31–43, Aug. 2015.

[4] S. Fang, Y. Wang, B. Gou and Y. Xu, "Toward future green maritime transportation: an overview of seaport microgrids and all-electric ships," *IEEE Trans. Veh. Technol*., vol. 69, no. 1, pp. 207-219, Jan. 2020.

[5] P. Krata, J. Szlapczynska, "Ship weather routing optimization with dynamic constraints based on reliable synchronous roll prediction," *Ocean Eng.*, vol. 150, pp. 124-137, Feb. 2018.

[6] R. Zaccone, E. Ottaviani, M. Figari, et al, "Ship voyage optimization for safe and energy-efficient navigation: A dynamic programming approach," *Ocean Eng.*, vol. 153, pp. 215-224, Apr. 2018.

[7] K. Hein, Y. Xu, G. Wilson and A. K. Gupta, "Coordinated optimal voyage planning and energy management of all-electric ship with hybrid energy storage system," *IEEE Trans. Power Syst.*, vol. 36, no. 3, pp. 2355-2365, May 2021.

[8] F. D. Kanellos, G. J. Tsekouras and N. D. Hatziargyriou, "Optimal demand-side management and power generation scheduling in an all-electric ship," *IEEE Trans. Sustain. Energy*, vol. 5, no. 4, pp. 1166-1175, Oct. 2014.

[9] C. Shang, D. Srinivasan and T. Reindl, "Economic and environmental generation and voyage scheduling of all-electric ships," *IEEE Trans. Power Syst.*, vol. 31, no. 5, pp. 4087-4096, Sept. 2016.

[10] S. Fang, Y. Xu, "Multi-objective robust energy management for all-electric shipboard microgrid under uncertain wind and wave," *Int. J. Electr. Power Energy Syst*., vol. 117, pp. 105600, May 2020.

[11] S. Fang, Y. Xu, S. Wen, T. Zhao, H. Wang and L. Liu, "Data-driven robust coordination of generation and demand-side in photovoltaic integrated all-electric ship microgrids," *IEEE Trans. Power Syst.*, vol. 35, no. 3, pp. 1783-1795, May 2020

[12] S. Wen et al., "Coordinated optimal energy management and voyage scheduling for all-electric ships based on predicted shore-side electricity price," *IEEE Trans. Ind. Appl*., vol. 57, no. 1, pp. 139-148, Jan.-Feb. 2021.

[13] D. E. Olivares, C. A. Cañizares and M. Kazerani, "A centralized energy management system for isolated microgrids," IEEE Trans. Smart Grid, vol. 5, no. 4, pp. 1864-1875, July 2014.

[14] P. C. Olival, A. G. Madureira, M. Matos, "Advanced voltage control for smart microgrids using distributed energy resources," *Electr. Power Syst. Resear*, vol. 146, pp. 132-140, May 2017.

[15] P. -H. Huang, P. -C. Liu, W. Xiao and M. S. El Moursi, "A novel droop-based average voltage sharing control strategy for DC microgrids," *IEEE Trans. Smart Grid*, vol. 6, no. 3, pp. 1096-1106, May 2015.

[16] F. D. Kanellos, E. M. Volanis and N. D. Hatziargyriou, "Power management method for large ports with multi-agent systems*," IEEE Trans. Smart Grid*, vol. 10, no. 2, pp. 1259-1268, Mar. 2019

[17] Imai A, Chen H C, Nishimura E, et al, "The simultaneous berth and quay crane allocation problem," *Transport Res E-Log*, vol. 44, no. 5, pp. 900-920, Sept. 2008.

[18] C. J. Ting, K. C. Wu and H. Chou, "Particle swarm optimization algorithm for the berth allocation problem," *Expert Syst. Appl.*, vol. 41, no. 4, pp. 1543-1550, Mar. 2014.

[19] A. Agra and M. Oliveira, "MIP approaches for the integrated berth allocation and quay crane assignment and scheduling problem," *Eur. J. Oper. Res.*, vol. 264, no. 1, pp. 138-148, Jan. 2018.

[20] A. Mao, T. Yu, Z. Ding, et al, "Optimal scheduling for seaport integrated energy system considering flexible berth allocation," *Appl. Energy*, vol. 308, pp. 118386, Feb. 2022.

[21] Y. Zhang, C. Liang, J. Shi, et al, "Optimal port microgrid scheduling incorporating onshore power supply and berth allocation under uncertainty," *Appl. Energy*, vol. 313, pp. 118856, May 2022.

[22] X. Sun, J. Qiu, Y. Tao, Y. Yi and J. Zhao, "Distributed optimal voltage control and berth allocation of all-electric ships in seaport microgrids," *IEEE Trans. Smart Grid*, vol. 13, no. 4, pp. 2664-2674, July 2022.

[23] N. N. A. Bakar, N. Bazmohammadi, H. Çimen, et al, "Data-driven ship berthing forecasting for cold ironing in maritime transportation," *Appl. Energy*, vol. 326, pp. 119947, Nov. 2022.

[24] J. Yin, X. Peng, J. He, Q. Huo and T. Wei, "Energy management method of a hybrid energy storage system combined with the transportation-electricity coupling characteristics of ports," *IEEE Trans. Intell. Transp. Syst*, doi: 10.1109/TITS.2023.3303497.

[25] X. Sun and J. Qiu, "Hierarchically coordinated voltage control in seaport microgrids considering optimal voyage navigation of all-electric ships," *IEEE Trans. Transp. Elect.*, vol. 8, no. 2, pp. 2191-2204, June 2022.

[26] C. Ju, P. Wang, L. Goel and Y. Xu, "A two-layer energy management system for microgrids with hybrid energy storage considering degradation costs," *IEEE Trans. Smart Grid*, vol. 9, no. 6, pp. 6047-6057, Nov. 2018.

[27] Z. Wang, H. Chen, J. Wang and et al, "Inverter-less hybrid voltage/var control for distribution circuits with photovoltaic generators," *IEEE Trans. Smart Grid*, vol. 5, no. 6, pp. 2718-2728, Nov. 2014.

[28] T. Ding, S. Liu, W. Yuan, Z. Bie and B. Zeng, "A two-stage robust reactive power optimization considering uncertain wind power integration in active distribution networks," *IEEE Trans. Sustain. Energy*, vol. 7, no. 1, pp. 301-311, Jan. 2016.

[29] S. Papathanassiou, N. Hatziargyriou, K. Strunz. "A benchmark low voltage microgrid network," *Proceedings of the CIGRE symposium: power systems with dispersed generation. CIGRE*, 2005: 1-8.

[30] S. H. Dolatabadi, M. Ghorbanian, P. Siano and N. D. Hatziargyriou, "An enhanced IEEE 33 bus benchmark test system for distribution system studies," *IEEE Trans. Power Syst.*, vol. 36, no. 3, pp. 2565-2572, May 2021.

Xianzhuo Sun received his B.Eng. degree in electrical engineering from Taiyuan University of Technology, M.E. degree in electrical engineering from Shandong University, and Ph.D. in electrical engineering from the University of Sydney in 2016, 2019 and 2023 respectively. He is currently working as the Postdoctoral Fellowship with Hong Kong Polytechnic University. His research interests include power system operation and voltage control, machine learning, electrical vehicles, all-electric ships, etc.

Jing Qiu (SM'22) is currently a Senior Lecturer in Electrical Engineering at the University of Sydney, Australia. He obtained his B.Eng. degree in control engineering from Shandong University, China, M.Sc. degree in environmental policy and management, majoring in carbon financing in the power sector, from The University of Manchester, U.K., and Ph.D. in electrical engineering from The University of Newcastle, Australia, in 2008, 2010 and 2014 respectively. His areas of interest include power system planning, data-driven energy market analysis, and artificial intelligence (AI)-assisted energy pricing and trading strategies. He is the Editorial Board Member of IET Renewable Power Generation and Energy Conversion and Economics.

Yuechuan Tao received the B.Sc. degree in Electrical Engineering and Automation from Shanghai Normal University, Shanghai, China, in 2017, and an M.Sc. degree in Electrical Engineering from the University of Sydney, Australia in 2019, and a Ph.D. degree in the University of Sydney, Australia. Currently, he is the wallenberg-ntu presidential postdoctoral fellow in Nanyang Technological University. His main fields of interest include power system operation and planning, electric vehicles, data-driven, smart grid, etc.

Huichuan Liu received the Master's degree in Electrical Engineering from The University of Sydney, Australia in 2018. He is currently pursuing the Ph.D. degree in Electrical Engineering at the University of Sydney, Australia. His research interests include power system operation and planning, distributed energy resources integration, electricity market, converter-dominated power system stability and AI application in energy systems.

Junhua Zhao (Senior Member, IEEE) received the Ph.D. degree in electrical engineering from the University of Queensland, Brisbane, QLD, Australia, in 2007. He was a Senior Lecturer with the University of Newcastle, and also with the Center for Intelligent Electricity Networks (CIEN), University of Newcastle, Australia. He is currently the Assistant Dean and Associate Professor with the School of Science and Engineering, The Chinese University of Hong Kong, Shenzhen, China. He is also the Director of the Energy Market and Finance Lab, Shenzhen Finance Institute, The Chinese University of Hong Kong. His research interests include power system analysis and computation, smart grid, electricity market, data mining, and artificial intelligence. Dr. Zhao received the "Young Scientist of the Future" award from ADC Forum in 2016, the IEEE PES General Meeting Best Paper Award in 2014, and the Science and Technology Progress Award (second prize) from the Hunan Provincial government, China, in 2013. He is the Editorial Board Member of IET Energy Conversion and Economics and Electric Power components and Systems.